Au Nanoparticle-Enhanced Surface Plasmon Resonance Sensing of Biocatalytic Transformations

Maya Zayats, Svetlana P. Pogorelova, Andrei B. Kharitonov, Oleg Lioubashevski, Eugenii Katz, and Itamar Willner*[a]

Abstract: *N*-(3-Aminopropyl)-*N*′-methyl-4,4′-bipyridinium is coupled to tiopronin-capped Au nanoparticles (diameter ca. 2 nm) to yield methyl(aminopropyl)viologen-functionalized Au nanoparticles ($MPAV^{2+}$-Au nanoparticles). In situ electrochemical surface plasmon resonance (SPR) measurements are used to follow the electrochemical deposition of the bipyridinium radical cation modified Au nanoparticles on an Au-coated glass surface and the reoxidation and dissolution of the bipyridinium radical cation film. The $MPAV^{2+}$-functionalized Au nanoparticles are also employed for the amplified SPR detection of NAD^+ and NADH cofactors. By SPR monitoring the partial biocatalyzed dissolution of the bipyridinium radical cation film in the presence of diaphorase (DP) NAD^+ is detected in the concentration range of 1×10^{-4} M to 2×10^{-3} M. Similarly, the diaphorase-mediated formation of the bipyridinium radical cation film on the Au-coated glass surface by the reduction of the $MPAV^{2+}$-functionalized Au nanoparticles by NADH is used for the amplified SPR detection of NADH in the concentration range of 1×10^{-4} M to 1×10^{-3} M.

Keywords: bioelectrocatalysis · biosensors · gold nanoparticles · NAD^+/NADH cofactors · surface plasmon resonance

Introduction

Surface plasmon resonance (SPR) is a versatile method to probe and characterize chemical changes on thin films of noble metal surfaces such as Au or Ag. The assembly of monolayers or thin films on SPR-active surfaces, as well as chemical reactions occurring on the surfaces, can be monitored by SPR spectroscopy. Accordingly, SPR has become a general technique for the characterization of the optical and structural features (e.g., refractive index or thickness) of thin films on surfaces.[1] Alternatively, SPR spectroscopy has also proven to be a useful analytical tool for the detection of recognition and binding processes on surfaces, and has been applied in many sensing systems.[2] Protein–protein binding interactions,[3,4] DNA–nucleic acid hybridization,[5] photochemically triggered binding and dissociation of antibodies to and from low molecular weight antigen monolayers, respectively,[6] or the swelling of imprinted polymers as a result of binding of the imprinted substrate[7] represent some of the detection systems reported. In most of the systems that involve SPR as a means of characterization or sensing, the chemical modification of the metal surface alters the refractive index and thickness of the surface, resulting in changes in the angle-dependent attenuated total reflectance.

The use of the SPR method is, however, hindered by the fact that the changes in the refractive index as a result of binding processes are often small, and so the systems display limited sensitivities. Enhanced sensitivities in SPR analyses have been reported through the association of macromolecular tags such as liposomes,[8] latex particles,[9] or proteins[10] to the recognition complexes on surfaces, thus increasing the changes in the refractive index at the sensing interface.

An interesting approach to the enhancement of SPR sensing processes involves the use of Au nanoparticles as labels. The possibility of synthesizing metal nanoparticles of controlled size and surface capping[11] allows the generation of low molecular weight- or biomaterial-Au nanoparticle conjugates. Specifically, the electronic coupling between the localized surface plasmons of the Au nanoparticles and the plasmon wave associated with the surface leads to enhanced shifts of the resonance angles.[12,13] Indeed, significant enhancement in the SPR changes has been reported upon the labeling of antigen–antibody complexes[14] or double-strand-

[a] Prof. Dr. I. Willner, M. Zayats, S. P. Pogorelova, Dr. A. B. Kharitonov, O. Lioubashevski, Dr. E. Katz
Institute of Chemistry and
The Farkas Center for Light-Induced Processes
The Hebrew University of Jerusalem
Jerusalem 91904, Israel
Fax: (+972) 2-652-7715
E-mail: willnea@vms.huji.ac.il

© 2003 Wiley-VCH Verlag GmbH & Co. KGaA, Weinheim
DOI: 10.1002/chem.200305104

ed DNA assemblies[15] with Au nanoparticles. Here we report on the use of bipyridinium-functionalized Au nanoparticles as active components for the amplified SPR analysis of biocatalytic processes. We demonstrate that the electrochemical or biocatalyzed deposition of bipyridinium radical cation-functionalized Au nanoparticles on Au surfaces enables enhanced SPR analysis of the NADH or NAD^+ cofactors in the presence of diaphorase.

Results and Discussion

Surface plasmon resonance spectroscopy has recently been applied to probe the electrochemical activation of redox-active films associated with Au surfaces.[16,17] The changes in the refractive indexes of the films in their different redox states, and possible swelling or shrinking processes associated with the redox states of the films, were monitored by SPR spectroscopy. The reversible redox-induced precipitation and dissolution of a film onto and from an Au electrode, respectively, could similarly lead to the SPR transduction of the electrochemical processes. Electrochemical reduction of bipyridinium salts, specifically of bipyridinium components tethered with long hydrophobic chains, yields bipyridinium radical cations that adsorb onto electrode surfaces[18]. Accordingly, the in situ electrochemical SPR analysis of the electrochemical reduction of methyl(aminopropyl)viologen ($MPAV^{2+}$) was examined (Figure 1). The minimum reflectivity angle of the SPR spectrum obtained upon application of a potential of −0.85 V for 5 min to an Au electrode in the presence of the solution of the bipyridinium salt is shifted by $\Delta\theta = 0.25°$, relative to the SPR spectrum of the system under an applied potential of −0.40 V. At this potential, the bipyridinium salt is reduced to the radical cation, and the product accumulated on the surface alters the reflectivity angle. The change in the minimum reflectivity angle as a result of the precipitation of the bipyridinium radical cation is, however, relatively small. In our study, we aim to detect minute changes in the surface-associated bipyridinium radical cation as a result of a coupled biocatalyzed transformations (vide infra). The small changes in the SPR spectrum of the surface that includes the bipyridinium radical cation film, do not enable the sensitive detection of the changes in the surface composition as a result of the biocatalytic process. We thus decided to employ bipyridinium-functionalized Au nanoparticles to amplify the changes in the angle of reflectance on the Au surface (Scheme 1). The

Figure 1. SPR spectra in the presence of $MPAV^{2+}$, 5×10^{-6} M, upon the application of the potentials of: a) −0.40 V and b) −0.85 V. The background electrolyte solution is composed of phosphate buffer 0.1 M, pH 7.0, under argon.

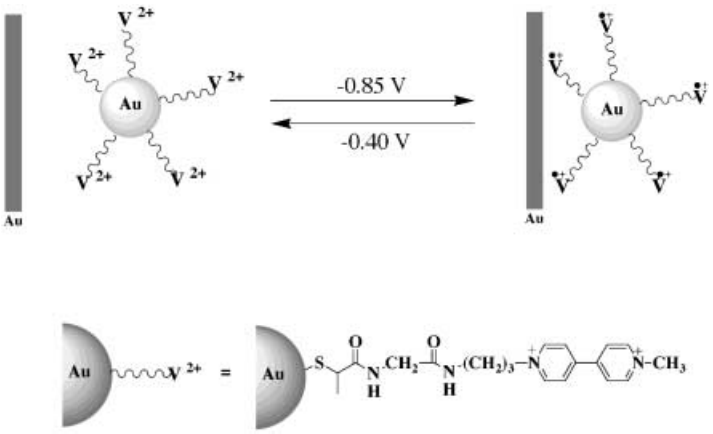

Scheme 1. Electrochemically controlled adsorption and desorption of the viologen-functionalized Au nanoparticles onto and from a SPR electrode interface, respectively.

tiopronin-functionalized Au nanoparticles were prepared by the method reported by Murray et al.[19] Tiopronin-modified Au nanoparticles were coupled to *N*-(3-aminopropyl)-*N*′-methyl-4,4′-bipyridinium (methyl(3-aminopropyl)viologen, $MPAV^{2+}$)".[20] Figure 2 shows the cyclic voltammogram of the methyl(aminopropyl)viologen-functionalized ($MPAV^{2+}$-functionalized) Au nanoparticles. Methyl(aminopropyl)viol-

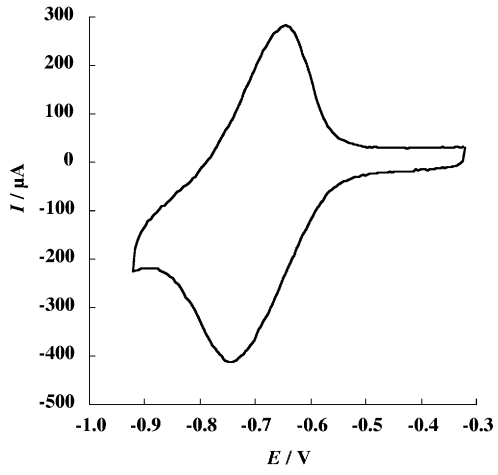

Figure 2. Cyclic voltammogram of the $MPAV^{2+}$-functionalized Au nanoparticles (0.3 mg mL^{-1}) recorded at the SPR-Au electrode. The background electrolyte solution is composed of phosphate buffer 0.1 M, pH 7.0, under argon. Potential scan rate: 6 V s^{-1}.

 © 2003 Wiley-VCH Verlag GmbH & Co. KGaA, Weinheim

ogen displayed electrochemical behavior typical of the 4,4′-bipyridinium units, with one couple of the redox peaks due to quasi-reversible one-electron reduction ([viologen]$^{2+/+\cdot}$, $E^{\circ\prime} = -0.68$ V, peak-to-peak separation $\Delta E = 110$ mV at the potential scan rate 6 V s^{-1}). (This high scan rate was applied in order to minimize the interference of traces of oxygen on the electrochemistry of the bipyridinium radical cation). The tiopronin-functionalized Au particles exhibit a narrow size distribution, with a mean diameter of approximately 2 nm (Figure 3). It should be noted that after coupling of the

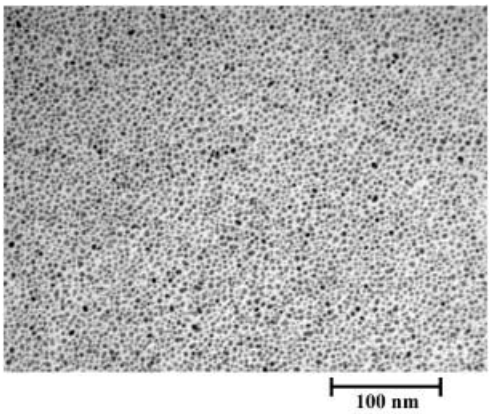

Figure 3. Transmission electron micrograph of the MPAV^{2+}-functionalized Au nanoparticles.

MPAV^{2+} to the tiopronin-modified Au nanoparticles, aggregates of the particles are observed. These presumably originate from the electrostatic crosslinking of the negatively charged particle by the positively charged bipyridinium units. Electrochemical quartz crystal microbalance experiments enabled us to estimate the coverage of the Au nanoparticles by the MPAV^{2+} units. In these experiments the bipyridinium radical cation-functionalized Au nanoparticles were deposited on the electrode of an Au quartz crystal under constant potential electrolysis (−0.85 V) under argon, and the charge passed through the system was followed in parallel with the monitoring of the frequency changes of the quartz crystal. Knowing the charge passed through the system (5.76×10^{-2} Coulombs), and from the frequency change of the quartz crystal, we estimate the total coverage of the Au electrode surface with the bipyridinium units and the Au nanoparticles to be 9.4×10^{-7} mol cm^{-2} and 2.5×10^{-8} mol cm^{-2}, respectively. This implies that approximately 38 ± 2 units of bipyridinium groups are associated with each Au nanoparticle. This value is in good agreement with the loading of similar bipyridinium-functionalized Au nanoparticles reported by Murray et al.[20]

Figure 4 A shows the SPR spectrum of the Au film in the presence of the bipyridinium-modified Au nanoparticles in the solution (curve a) and the SPR spectrum of the interface after the electrochemical deposition of the bipyridinium radical cation-modified Au nanoparticles on the Au surface upon application of a potential of −0.85 V to the Au electrode (curve b). Clearly, the electrochemical deposition of the labeled Au nanoparticles onto the Au electrode results

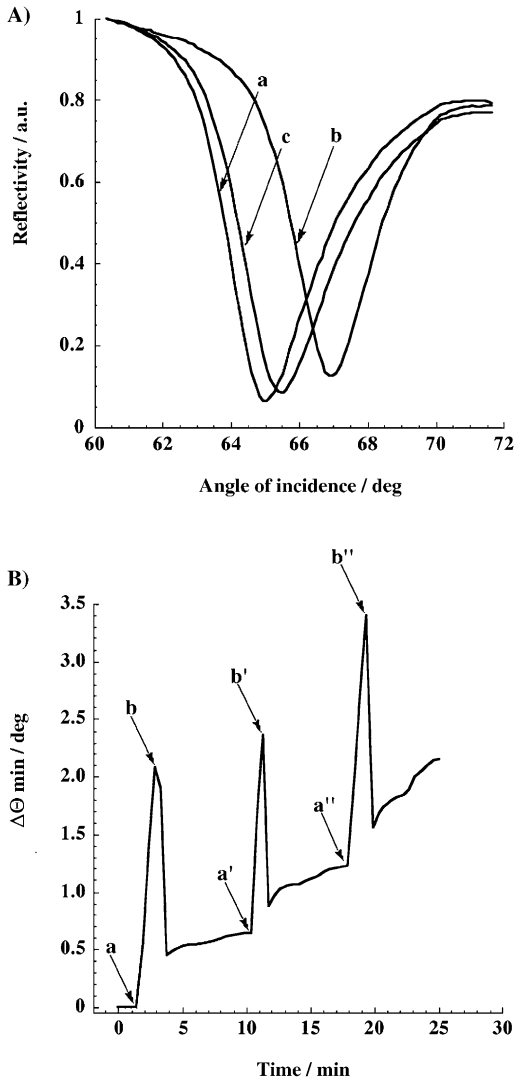

Figure 4. The SPR detection of the electrochemically controlled reversible deposition of the bipyridinium radical cation-modified Au nanoparticles on the gold-coated SPR-active electrode. A) SPR spectra recorded in the presence of the MPAV^{2+}-functionalized Au nanoparticles (0.3 mg mL^{-1}) upon application of potentials of: a) −0.40 V, b) −0.85 V, and c) again −0.40 V. The spectra were recorded after the application of the respective potentials for 5 min. B) The time-dependent changes in the minimum reflectance angles (sensogram) recorded in the presence of the MPAV^{2+}-functionalized Au nanoparticles (0.3 mg mL^{-1}) upon application of the potentials: a) −0.85 V, and b) −0.40 V. The cyclic application of the respective potentials was continued repeatedly (a′b′ and a″b″). The background electrolyte solution was composed of phosphate buffer 0.1 M, pH 7, under argon.

in a significant shift in the minimum reflectivity angle: $\Delta\theta = 2.5°$. Thus, while only small changes in the minimum reflectivity angle are observed upon the electrochemical reduction of the unlabeled bipyridinium salt and the deposition of the radical cation, the generation of the bipyridinium–Au nanoparticle conjugate enhances the changes in the minimum reflectance angle. The enhanced shift in the SPR spectrum observed upon formation of the bipyridinium radical cation–Au nanoparticle film may be attributed to the plasmon–plasmon coupling between the nanoparticles and the Au surface. Partial charging of the Au nanoparticles by

© 2003 Wiley-VCH Verlag GmbH & Co. KGaA, Weinheim

the transfer of electrons from the bipyridinium radical cation may enhance this electronic coupling and leads to the observed shift. Application of a potential corresponding to −0.4 V on the electrode, resulting in the oxidation of the bipyridinium radical cation, leads to a decrease in the minimum reflectivity angle, although the original minimum reflectivity angle of the bare gold surface is not reached (Figure 4A, curve c). Similarly to the recent efforts to probe the redox reactions of thin films associated with Au surfaces by means of SPR spectrometry,[16,17] we examined the electrochemical deposition and dissolution of the bipyridinium radical cation–Au nanoparticle conjugate onto and from the gold film, respectively, through the cyclic SPR readout (Figure 4B). It is evident that upon the reduction of the bipyridinium–nanoparticle conjugate ($E = -0.85$ V), a change of approximately $\Delta\theta = 2.5°$ in the minimum reflectivity angle is observed. Upon the application of the potential that oxidizes the bipyridinium radical cation ($E = -0.4$ V), the minimum reflectivity angle of the interface does not return to the original value and a residual change of approximately $\Delta\theta = 0.5°$ is observed. Each deposition/dissolution cycle of the bipyridinium radical cation/Au nanoparticle conjugate further increases the residual change in the minimum reflectivity angle by approximately 0.3–0.5°.

Bipyridinium radical cations ($V^{+\cdot}$) reduce NAD^+ in the presence of diaphorase (DP)[21] according to Equation 1. From the thermodynamic redox potentials of the two components, the equilibrium constant $K_{eq} = 2.5 \times 10^4$ is calculated for the process.

$$2\,V^{+\cdot} + NAD^+ + H^+ \overset{DP}{\rightleftharpoons} 2\,V^{2+} + NADH \qquad (1)$$

Thus, the bipyridinium-functionalized Au nanoparticles were used as labels for the amplified detection of the NAD^+ cofactor by the use of SPR spectroscopy as the readout method (Scheme 2). The Au-coated glass slide was subjected to a potential of −0.85 V for 100 minutes. (The relatively long time interval for electrolysis is due to the low bulk concentration of the bipyridinium-functionalized Au nanoparticles.) Under these conditions, the $V^{+\cdot}$-Au nanoparticles are deposited on the electrode. The sensogram corresponding to the changes in the minimum reflectivity angles as a function of time is depicted in Figure 5A. It is evident that the shifts in the minimum reflectivity angle values reach a saturation value after approximately 80 minutes. This implies that the charge transport through the film becomes inefficient as the thickness of the $V^{+\cdot}$-Au nanoparticles layer increases. Simultaneously with the recording of the sensogram shown in Figure 5A, the charge passed through the system, resulting in the deposition of the bipyri-

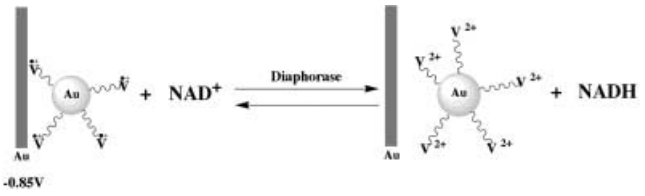

Scheme 2. Biocatalytic equilibrium established at the SPR electrode functionalized with the Au nanoparticle-bipyridinium radical cation film and in the presence of NAD^+ and diaphorase (DP) upon the application of a reducing potential of −0.85 V on the electrode.

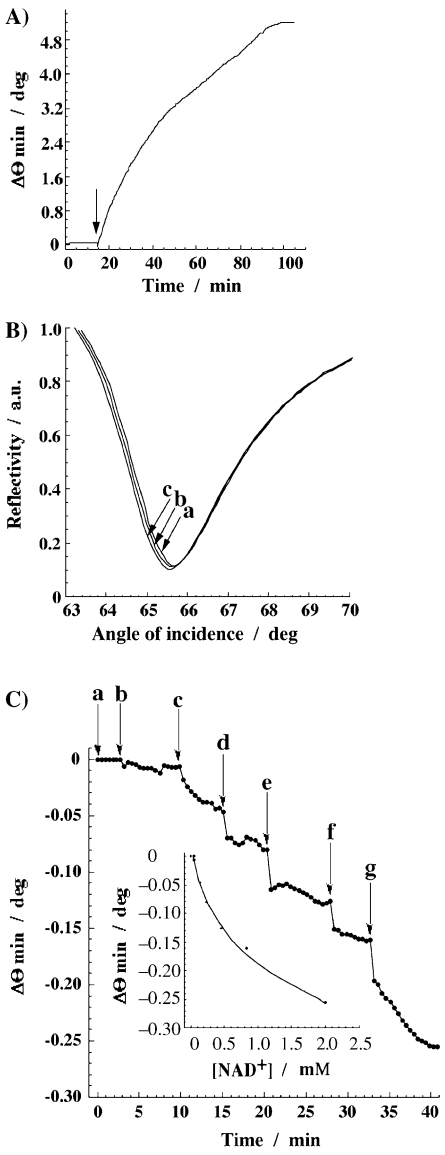

Figure 5. The amplified SPR detection of the bioelectrocatalytic reduction of NAD^+ by the Au nanoparticle–bipyridinium radical cation interface associated with the electrode in the presence of diaphorase. A) The time-dependent changes in the minimum reflectance angles (sensogram) recorded in the presence of the $MPAV^{2+}$-functionalized Au nanoparticles (0.3 mg mL^{-1}) upon the application of the potential of −0.85 V. The arrow shows the time when the potential was applied on the electrode. B) The SPR spectra recorded in the presence of diaphorase (6 mg mL^{-1}) and different concentrations of NAD^+: a) 0 M, b) 2.4×10^{-4} M, and c) 8.4×10^{-4} M. C) The time-dependent changes in the minimum reflectance angles (sensogram) recorded in the presence of the $MPAV^{2+}$-functionalized Au nanoparticles (0.3 mg mL^{-1}) and diaphorase (6 mg mL^{-1}) and the applied potential of −0.85 V upon addition of different concentrations of NAD^+: a) 5×10^{-5} M, b) 6×10^{-5} M, c) 1.5×10^{-4} M, d) 2.4×10^{-4} M, e) 4.5×10^{-4} M, f) 8.4×10^{-4} M, and g) 2×10^{-3} M. Inset: The calibration curve corresponding to the changes in the minimum reflectance angle as a function of NAD^+ concentration. All the measurements were performed in a background solution consisting of phosphate buffer 0.1 M, pH 7.0, under argon, upon application of the potential of −0.85 V.

 © 2003 Wiley-VCH Verlag GmbH & Co. KGaA, Weinheim

dinium radical cation, was monitored. Knowing the total coverage of the bipyridinium units linked to the surface, and that the average loading of each particle is 38 ± 2 units of $MPAV^{2+}$, we estimate that approximately 2.5×10^{-8} mol cm^{-2} Au nanoparticles are associated with the Au-coated glass support employed in the biocatalytic SPR experiments. The loading of the Au electrode with the reduced $MPAV^{2+}$-functionalized Au nanoparticles, calculated from the electrochemical quartz crystal microbalance experiments, corresponds to the mean thickness of the layer: approximately 140 nm. The analysis of NAD^+ is performed under conditions in which the $V^{+\cdot}$-Au nanoparticle film reaches the saturation loading, and NAD^+ is added to the system, in the presence of DP as biocatalyst, in which the potential of -0.85 V is applied on the electrode and the V^{2+}-Au nanoparticles are present in the electrolyte solution. Figure 5B shows the SPR spectra of the Au surface after the electrochemical deposition of the $V^{+\cdot}$-Au nanoparticle film (curve a), and as a result of the addition of NAD^+ (2.4×10^{-4} M; curve b, 8.4×10^{-4} M; curve c) in the presence of DP. Control experiments indicate that no changes in the SPR spectra of the surface-associated bipyridinium radical cation film are observed upon the addition of only NAD^+ or DP. Clearly, the addition of NAD^+ and DP shifts the minimum reflectivity angle to lower values, implying that the addition of NAD^+ resulted in the partial dissolution of the film. This is consistent with the sequence of biocatalyzed and electrochemical reactions depicted in Scheme 2. Addition of NAD^+ in the presence of DP results in the reduction of the NAD^+ cofactor to NADH and the partial dissolution of the film associated with the surface. The existence of the V^{2+}-Au nanoparticles in the electrolyte solution prohibits the dissolution of the entire film from the electrode surface. Furthermore, since the electrode is biased at -0.85 V the reduction of the V^{2+}-Au nanoparticles proceeds to regenerate the film associated with the electrode. Thus, the addition of NAD^+ to the system yields a steady-state equilibrium in which all of the species depicted in Scheme 2 are present in the system. The formation of this equilibrium results in the partial dissolution of the film, consistently with the decrease in the value of the minimum reflectivity angle of the interface. Also, the reactions outlined in Scheme 2 suggest that the elevation of the NAD^+ concentration in the system should increase the extent of the reoxidation and dissolution of the $V^{+\cdot}$-Au nanoparticle film. Thus, as the concentration of NAD^+ in the system is higher, the minimum reflectivity angle should shift to lower values and should resemble the SPR spectrum of the bare Au interface. Figure 5C shows the sensogram that corresponds to the changes in the minimum reflectivity angles in the presence of variable concentrations of NAD^+. The minimum reflectivity angles of the modified film decrease with higher concentration of NAD^+ in the system. Figure 5C (inset) shows the derived calibration curve. Clearly, in situ electrochemical SPR spectroscopy enables the detection of NAD^+ in the concentration range of 1×10^{-4} M to 2×10^{-3} M through the use of bipyridinium-functionalized Au nanoparticles as a signal enhancement label. It should be noted that the minute changes in the SPR spectrum of the Au interface upon the electrochemical deposition of the unlabeled bipyridinium radical cation film prohibit the use of the unlabeled film as an active interface for the SPR detection of NAD^+.

Since the DP-biocatalyzed reduction of NAD^+ by the $V^{+\cdot}$-Au nanoparticle film is reversible, one may examine the reverse reaction, which involves the DP-catalyzed reduction of the V^{2+}-Au nanoparticles by NADH, and thus use the surface-deposited $V^{+\cdot}$-Au particle as a label for the enhanced SPR detection of NADH (Scheme 3). According to this scheme, no potential is applied on the electrode, and the chemical deposition of the $V^{+\cdot}$-Au nanoparticles occurs on the surface as a result of the reaction between the functionalized particles and NADH in the presence of DP. The amount of deposited $V^{+\cdot}$-Au nanoparticles increases with higher concentration of NADH. Note, however, that for every NADH concentration a different steady-state content of $V^{+\cdot}$-Au nanoparticles will be deposited on the surface, due to the equilibrium features of the process (Eq. 1). Figure 6A shows the SPR spectra of the system that includes the V^{2+}-Au nanoparticles and DP prior to the addition of NADH (curve a), and after the addition of NADH (1.5×10^{-4} M; curve b, and 8.4×10^{-4} M; curve c). Upon the addition of NADH, the minimum reflectivity angle is shifted to higher values, consistently with the formation of the precipitate of the $V^{+\cdot}$-Au nanoparticles on the surface. Figure 6B shows the sensogram corresponding to the changes in the minimum reflectivity angles upon the addition of variable concentrations of NADH. As the concentration of NADH is elevated, the changes in the minimum reflectivity angles are indeed higher. Figure 6B (inset) depicts the derived calibration curve. The NADH is detected in the concentration range of 1×10^{-4} M to 1.5×10^{-3} M. It should be noted that no significant changes in the minimum reflectivity angle of the interface are observed upon the reaction of the unlabeled bipyridinium salt of V^{2+} with NADH in the presence of DP. Thus, the labeling of the resulting $V^{+\cdot}$ film with the Au-particles is essential to enhance the differences in the SPR reflectance angles.

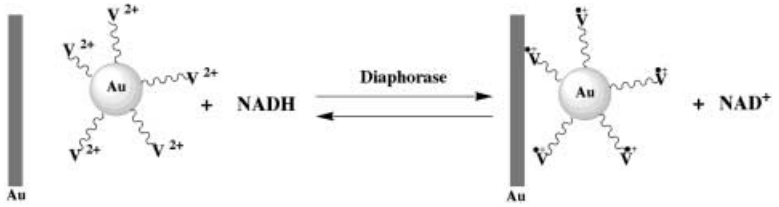

Scheme 3. Biocatalytic equilibrium established at the SPR electrode interface in the presence of the bipyridinium-modified Au nanoparticles, NADH, and diaphorase (DP).

© 2003 Wiley-VCH Verlag GmbH & Co. KGaA, Weinheim

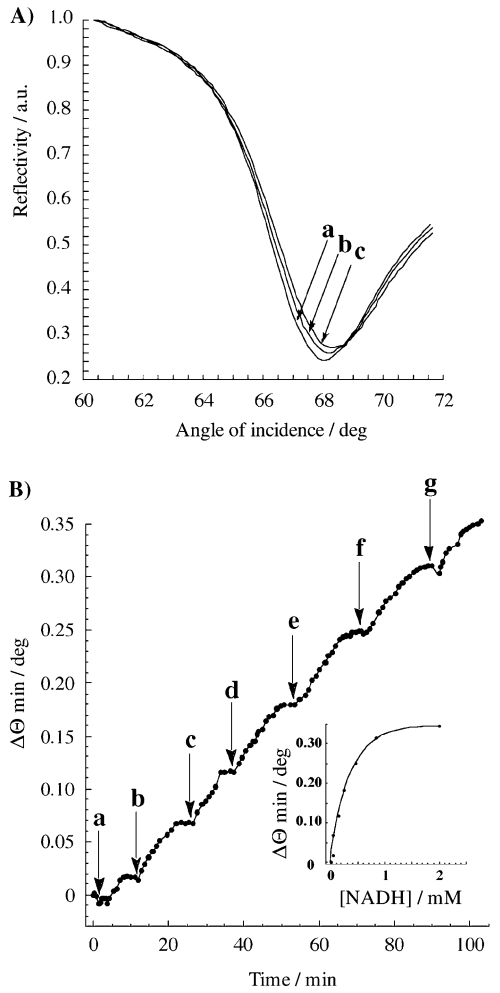

Figure 6. The amplified SPR detection of the biocatalytic oxidation of NADH in the presence of the bipyridinium-functionalized Au nanoparticles and diaphorase. A) SPR spectra recorded in the presence of the $MPAV^{2+}$-functionalized Au nanoparticles (0.3 mg mL^{-1}), diaphorase (6 mg mL^{-1}), and different concentrations of NADH: a) 0 M, b) 1.5×10^{-4} M, and c) 8.4×10^{-4} M. B) The time-dependent changes in the minimum reflectance angles (sensogram) recorded in the presence of the $MPAV^{2+}$-functionalized Au nanoparticles (0.3 mg mL^{-1}) and diaphorase (6 mg mL^{-1}) upon addition of different concentrations of NADH: a) 5×10^{-5} M, b) 6×10^{-5} M, c) 1.5×10^{-4} M, d) 2.4×10^{-4} M, e) 4.5×10^{-4} M, f) 8.4×10^{-4} M, and g) 2×10^{-3} M. Inset: The calibration curve corresponding to the changes in the minimum reflectance angle as a function of NADH concentration. All the measurements were performed in a background solution consisting of a phosphate buffer 0.1 M, pH 7.0, under argon.

Conclusion

This study has demonstrated the use of bipyridinium-functionalized Au nanoparticles for the in situ electrochemical SPR detection of NAD^+ and for the chemically induced SPR detection of the reduced cofactor NADH. The gold nanoparticles enhance the changes in the SPR reflectance angles of the surface-deposited bipyridinium radical cation–Au nanoparticle films in the two systems. Previous studies employed static Au nanoparticles associated with molecular or biomolecular interfaces linked to surfaces as labels for enhancing the changes in the reflectance angles in the SPR spectra. In this study we demonstrate the novel application of functionalized Au nanoparticles as active components that are deposited or eliminated from the surface in the course of the amplified detection of the NAD^+ or NADH cofactors. The sensing of the NAD^+ and NADH cofactors is of substantial interest[22] due to the numerous biocatalytic transformations that involve NAD^+- or NADH-dependent enzymes. This article introduces a new concept for the enhanced SPR analyses of these different biocatalyzed transformations.

Experimental Section

Chemicals: The tiopronin monolayer-capped gold nanoparticles were prepared as described in the literature.[19] *N*-Methyl-*N*′-(3-aminopropyl)-4,4′-bipyridinium dinitrate, methyl(aminopropyl)viologen ($MPAV^{2+}(NO_3^-)_2$) was synthesized by the published procedure.[23] Ion exchange of the halide counterions to produce the dinitrate salt was performed as described before.[24] Coupling of methyl(aminopropyl)viologen to tiopronin monolayer-protected gold nanoparticles was performed as described by Murray et al.[20] 2-(*N*-Morpholino)ethanesulfonic acid (MES) buffer, 1-[3-(dimethylamino)propyl]-3-ethylcarbodiimide hydrochloride (EDC), and *N*-hydroxysulfosuccinimide sodium salt (NHS, $HAuCl_4\cdot3H_2O$), *N*-(2-mercaptopropionyl)glycine (tiopronin), sodium borohydride, methyl iodide, 4,4′-bipyridine, 3-bromopropylamine, and tetrabutylammonium nitrate were purchased from Sigma and Aldrich and were used as supplied. Diaphorase (E.C. 1.8.1.4., from *Clostridium kluyveri*) and nicotinamide adenine dinucleotide cofactors, both the oxidized (NAD^+) and reduced (NADH) forms, were purchased from Sigma. Ultrapure water from Barnstead NANOpure Diamond system was used in all the experiments.

In situ electrochemical SPR measurements: The surface plasmon resonance (SPR) Kretschmann-type Biosuplar-2 spectrometer (Analytical-μSystem, Germany) with a light-emitting diode light source, $\lambda = 670$ nm, prism refraction index ($n = 1.61$) and a dynamic angle range (up to 19° in air) was used in this work. The SPR data were processed with the aid of Biosuplar-2 software (2.2.30). The SPR sensograms represent real-time changes in the minimum reflectivity angle and were recorded by the use of a home-built flow cell. Multi-potential step chronoamperometry experiments were performed with an electrochemical analyzer (EG&G, VersaStat) linked to a computer (EG&G Software #270/250). Glass supports (20×20 mm) covered with a chromium sub-layer (≈5 nm) and a gold layer (≈50 nm) supplied by Analytical-μSystem, were used for the SPR measurements. The gold-covered glass plate was used as a working electrode (1.5 cm^2 area exposed to the solution), an auxiliary Pt and a quasi-reference Ag electrode were made from wires of 0.5 mm diameter and added to the cell. The Ag quasi-reference electrode was calibrated[25] according to the potential of dimethylviologen ($E^\circ = -0.687$ V versus saturated calomel electrode (SCE)), measured by cyclic voltammetry and the potentials are reported versus SCE. The SPR sensograms (time-dependent changes in the reflectance minimum) were measured in situ upon application of an external potential onto the working electrode.

In situ electrochemical QCM measurements: A QCM analyzer (Fluke 164T multifunctional counter, 1.3 GHz, TCXO) linked to a computer by homemade software was used for microgravimetric measurements. Quartz crystals (AT-cut, approximately 9 MHz, EG&G) sandwiched between two Au electrodes (geometrical area 0.2 cm^2, roughness factor ca. 3.5) were used. The Au electrodes associated with the QCM crystal were applied for in situ electrochemical microgravimetric measurements.

Acknowledgment

This research is supported by the German-Israeli Program (DIP). M.Z. acknowledges the Levi Eshkol fellowship, the Ministry of Science, Israel.

 © 2003 Wiley-VCH Verlag GmbH & Co. KGaA, Weinheim

[1] a) T. Liebermann, W. Knoll, *Colloids Surf. Part A* **2000**, *171*, 115–130; b) W. Knoll, *Annu. Rev. Phys. Chem.* **1998**, *49*, 569–638; c) A. G. Frutos, R. M. Corn, *Anal. Chem.* **1998**, *70*, 449A–455A.
[2] a) J. M. Brockmann, B. P. Nelson, R. M. Corn, *Annu. Rev. Phys. Chem.* **2000**, *51*, 41–63; b) J. G. Quinn, S. O'Neill, A. Doyle, C. McAtamney, D. Diamond, B. D. MacCraith, R. O'Kennedy, *Anal. Biochem.* **2000**, *281*, 135–143; c) C. D. Xiao, S. F. Sui, *Sens. Actuators B* **2000**, *66*, 174–177.
[3] a) P. Schuck, *Annu. Rev. Biophys. Biomol. Struct.* **1997**, *26*, 541–566; b) S. Löfas, *Pure Appl. Chem.* **1995**, *67*, 829–834.
[4] a) S. Heyse, O. P. Ernst, Z. Dienes, K. P. Hofmann, H. Vogel, *Biochemistry* **1998**, *37*, 507–522; b) C. E. H. Berger, T. A. M. Beumer, R. P. H. Kooyman, J. Greve, *Anal. Chem.* **1998**, *70*, 703–706; c) J. Li, R. Cook, M. L. Doyle, P. Hensley, D. E. McNulty, I. Chaiken, *Proc. Natl. Acad. Sci. USA.* **1997**, *94*, 6694–6699; d) C. Lange, K. W. Koch, *Biochemistry* **1997**, *36*, 12019–12026.
[5] a) K. A. Peterlinz, R. M. Georgiadis, T. M. Heme, M. J. Tarlov, *J. Am. Chem. Soc.* **1997**, *119*, 3401–3402; b) F. Caruso, E. Rodda, D. N. Furlong, V. Haring, *Sens. Actuators B*, **1997**, *41*, 189–197; c) F. F. Bier, F. Kleinjung, F. W. Scheller, *Sens. Actuators B* **1997**, *38–39*, 78–82; d) A. J. Thiel, A. G. Frutos, C. E. Jordan, R. M. Corn, L. M. Smith, *Anal. Chem.* **1997**, *69*, 4948–4956.
[6] E. Kaganer, R. Pogreb, D. Davidov, I. Willner, *Langmuir* **1999**, *15*, 3920–3923.
[7] R. Gabai, N. Sallacan, V. Chegel, T. Bourenko, E. Katz, I. Willner, *J. Phys. Chem. B* **2001**, *105*, 8196–8202.
[8] T. Wink, S. J. van Zuilen, A. Bult, W. P. van Bennekom, *Anal. Chem.* **1998**, *70*, 827–832.
[9] a) E. F. A. de Vries, R. B. M. Schasfoort, J. van der Plas, J. Greve, *Biosens. Bioelectron.* **1994**, *9*, 509–514; b) S. Kubitschko, J. Spinke, T. Brückner, S. Pohl, H. Oranth, *Anal. Biochem.* **1997**, *253*, 112–122.
[10] a) C. E. Jordon, A. G. Frutos, A. J. Thiel, R. M. Corn, *Anal. Chem.* **1997**, *69*, 4939–4947; b) M. Zayats, O. A. Raitman, V. I. Chegel, A. B. Kharitonov, I. Willner, *Anal. Chem.* **2002**, *74*, 4763–4773.
[11] A. C. Templeton, M. P. Wuelfing, R. W. Murray, *Acc. Chem. Res.* **2000**, *33*, 27–36.
[12] a) L. A. Lyon, M. D. Musick, P. C. Smith, B. D. Reiss, D. J. Pena, M. J. Natan, *Sens. Actuators B* **1999**, *54*, 118–124; b) L. A. Lyon, D. J. Pena, M. J. Natan, *J. Phys. Chem. B* **1999**, *103*, 5826–5831.
[13] S. Chah, E. Hutter, D. Roy, J. H. Fendler, J. Yi, *Chem. Phys.* **2001**, *272*, 127–128.
[14] L. A. Lyon, M. D. Musick, M. J. Natan, *Anal. Chem.* **1998**, *70*, 5177–5183.
[15] L. He, M. D. Musick, S. R. Nicewarner, F. G. Sallinas, S. J. Benkovic, M. J. Natan, C. D. Keating, *J. Am. Chem. Soc.* **2000**, *122*, 9071–9077.
[16] a) V. Chegel, O. A. Raitman, E. Katz, R. Gabai, I. Willner, *Chem. Commun.* **2001**, 883–884; b) A. Baba, M. K. Park, R. A. Advincula, W. Knoll, *Langmuir* **2002**, *18*, 4648–4652; c) A. Baba, R. C. Advincula, W. Knoll, *J. Phys. Chem. B* **2002**, *106*, 1581–1587.
[17] a) O. A. Raitman, E. Katz, I. Willner, V. I. Chegel, G. V. Popova, *Angew. Chem.* **2001**, *113*, 3761–3764; *Angew. Chem. Int. Ed.* **2001**, *40*, 3649–3652; b) V. Chegel, O. A. Raitman, O. Lioubashevski, Y. Shirshov, E. Katz, I. Willner, *Adv. Mater.* **2002**, *14*, 1549–1553; c) O. A. Raitman, E. Katz, A. F. Bückmann, I. Willner, *J. Am. Chem. Soc.* **2002**, *124*, 6487–6496.
[18] C. L. Bird, A. T. Kuhn, *Chem. Soc. Rev.* **1981**, *10*, 49–82.
[19] A. C. Tempelton, S. Chen, S. M. Gross, R. W. Murray, *Langmuir* **1999**, *15*, 66–76.
[20] A. C. Templeton, D. E. Cliffel, R. W. Murray, *J. Am. Chem. Soc.* **1999**, *121*, 7081–7089.
[21] a) A. J. Fry, S. B. Sobolov, M. D. Leonida, K. I. Voivodov, *Tetrahedron Lett.* **1994**, *35*, 5607; b) H. C. Chang, T. Matsue, I. Uchida, T. Osa, *Chem. Lett.* **1989**, 1119; c) G. T. R. Palmore, H. Bertschy, S. H. Bergens, G. M. Whitesides, *J. Electroanal. Chem.* **1998**, *443*, 155–161.
[22] L. Gorton, E. Dominguez, *Rev. Mol. Biotechnol.* **2002**, 371–392.
[23] E. Katz, A. L. de Lacey, J. L. G. Fierro, J. M. Palacios, V. M. Fernandez, *J. Electroanal. Chem.* **1993**, *358*, 247–259.
[24] X. Tang, T. W. Schneider, J. W. Walker, D. A. Buttry, *Langmuir* **1996**, *12*, 5921–5933.
[25] E. Katz, D. D. Schlereth, H.-L. Schmidt, *J. Electroanal. Chem.* **1994**, *367*, 59–70.

Received: May 6, 2003
Revised: August 14, 2003 [F5104]

© 2003 Wiley-VCH Verlag GmbH & Co. KGaA, Weinheim